Numerical Evaluation of the Extinction Coefficient of Honeycomb Solar Receivers

Rami Elnoumeir*, Raffaele Capuano*, Thomas Fend‡*

*German Aerospace Center (DLR), Institute of Solar Research,

(rami.noumeir@gmail.com, raffaele.capuano@dlr.de)

‡ Corresponding Author; Thomas Fend, Linder Höhe, 51147 Köln, Tel: +49 2203 601 2101, Fax: +49 2203 601 4141,
thomas.fend@dlr.de

Abstract- Open volumetric receivers are porous media used in absorbing concentrated solar radiation reflected from a heliostat field with the objective to gain heat for an electricity generating thermal engine. Air is sucked through the hot, open porous material and heats up to high temperatures before it enters the steam generator of a turbine. In order to optimize these components in terms of pore geometry, a numerical prediction of the heat transfer and flow properties is useful. Due to the high complexity of the porous media's microstructure, effective parameters are used to describe the physical phenomena occurring in such structures on a macro-scale level. This study evaluates numerically one of the necessary parameters: the effective extinction coefficient. It describes how the concentrated radiation is absorbed in the volume of the receiver. For this purpose, a self-developed numerical tool in ANSYS environment has been used. The developed tool calculates the effective extinction coefficient of the solar radiation striking the receiver's inlet at any angle of incidence. Afterwards the tool can be applied for various honeycomb geometries and the generated coefficients may be used to predict the complete thermal behaviour of the receiver with the purpose to find a new geometry with a higher solar-to-thermal efficiency.

1. Introduction

In solar tower technology, a large number of controlled mirrors (heliostats) reflect the solar radiation onto a receiver fixed at the top of a tower. The concentrated solar radiation heats the receiver, which in turn exchange the absorbed thermal energy with a heat transfer fluid that is used to feed a conventional boiler of a steam turbine for electricity generation [1, 2, 3]. Tubular and volumetric receivers are two common examples used in solar towers. Volumetric receivers introduced in the late seventies [4], when compared with tube receivers, offer the advantage of radiation penetration into the volume of the receiver. The radiated power is spread over a volume instead of a surface area, leading to a lower average temperature of the receiver, and hence, less radiation is emitted to the atmosphere [1]. Therefore, the term "**volumetric**" is given to any absorber with effective area for solar absorption many times larger than that of the thermal radiation losses [5].

Volumetric absorbers are available in different materials and microstructures; foam ceramics, fibre mesh and extruded honeycomb ceramics represent some of the alternatives which can serve as solar absorbers [6]. To decide for any candidate receiver, it must guarantee a high absorption, high porosity and cell density, sustain high fluxes, have good air permeability and high thermal conductivity [7]. In general, a volumetric absorber is a porous medium that either has a complex microstructure (foams) or a geometric pattern (honeycombs). Therefore, studying its physical properties on the micro-scale level is computationally expensive. A continuum approach can therefore be used in analysing such a structure in order to predict its performance in application under operational environment with a reduced simulation time and memory requirement [8]. A continuum model treats the volume of interest on a macro-scale level, where effective parameters can describe in average the physical properties of the system over the volume. The microstructure of the porous medium is no longer of interest. On the other hand, effective parameters like porosity (P_0), that is the ratio between the void volume and the total volume of the porous structure, the extinction coefficient (β) that defines the attenuation of the radiation in such absorbers, the specific surface area (A_v), which is a measure for the availability of surface for heat exchange in porous materials, defined as the

ratio of the wet surface to the corresponding volume, and the convective heat transfer coefficient (h), defined as the ratio of the heat flux to the thermodynamic driving force are used in order to describe the physical phenomena occurring in such porous volumes [3], [9], [10]. This homogenous numerical approach has been taken by several research groups: Petrasch et al. [11], Caliot et al. [12] and Capuano et al. [2]. Effective parameters are always required in these numerical studies.

This study evaluates numerically the effective radiative parameter extinction coefficient (β) of the solar radiation ($\overline{G_0}$) striking a volumetric solar absorber module of honeycomb structure known from the so called HiTRec technology, an absorber made from a pattern of square-shape hollow channels used for the receiver of the Solar Tower Jülich [2]. To investigate this patterned volume, only a *single channel* of the module is studied, because it – as an elementary cell – represents the physical behaviour of the whole component. The effective parameter evaluated from this REV describes the attenuation of the solar radiation in the complete volume. This geometry remains the best choice for large-scale applications due to reduced production costs, easy manufacturability and acceptable performance. However, the geometry suffers from high radiative heat losses from the inlet zone. An innovative absorber geometry is therefore highly in demand. The numerical tool presented in this study is one of the necessary steps to achieve such geometry as it assesses a very important phenomenon occurring in a solar receiver: radiative behavior. While there has been already experimental work to evaluate the extinction coefficient (β) through transmittance measurements of different investigated samples [2], a specific numerical tool to evaluate that parameter was not available. The developed tool offers the ability of predicting an enhanced geometry through numerical modeling, enabling a deeper insight of the radiative behavior in the complete volume of honeycomb structures.

A novel honeycomb structure with modified cell geometry is investigated using the developed numerical tool. The comparison between the radiation attenuation in both geometries is presented at the end of the study. The developed tool is valid for the assessment of the extinction coefficient (β) of the solar radiation striking any honeycomb structure at any angle of incidence (θ). This evaluated radiative parameter (β) and all the other effective parameters of a solar absorber are used in a continuum model simulation to evaluate the overall thermal behaviour of any proposed honeycomb geometry during operation.

2. Materials and Methods

In a volumetric solar receiver, the solar flux ($\overline{G_{0-n}}$) striking the receiver's inlet at an angle of incidence (θ_n) will be attenuated in the porous material and can be represented by the following exponential law as stated in [13] and [14]:

$$G(z)_n = \overline{G_{0-n}}.\cos(\theta_n).P_0.e^{-\beta_n.z} \tag{1}$$

where

$$G_{0-n} = \overline{G_{0-n}}.\cos(\theta_n) \tag{2}$$

When "equation (1)" is differentiated with respect to (z), the volumetric radiative power source is obtained and given as:

$$\frac{dG(z)_n}{dz} = -G_{0-n}.P_0.\beta_n.e^{-\beta_n.z} \tag{3}$$

The purpose of this work is to develop a numerical tool that can evaluate the attenuation of the solar radiation penetrating honeycomb receivers at any angle of incidence (θ_n), and hence, evaluates the corresponding effective radiative parameter (β_n). An extinction coefficient ($\beta_{\sum n}$) considering for the attenuation of the total radiative flux shining on the inlet with different angles of incidence (15 angles in this study) is also deduced. In this case, "equation (1)" may be rewritten in the following form:

$$G(z)_T = \left[\sum_{n=1}^{15} G_{0-n}\right].P_0.e^{-\beta_{\sum n}.z} \tag{4}$$

and "equation (3)" can be rewritten as:

$$\frac{dG(z)_T}{dz} = -\left[\sum_{n=1}^{15} G_{0-n}\right].P_0.\beta_{\sum n}.e^{-\beta_{\sum n}.z} \tag{5}$$

with a total of 15 angles of incidence investigated.

Using the solar load model in ANSYS Fluent, an external solar beam with an angle of incidence (θ_n) and radiative flux density ($\overline{G_{0-n}}$) of choice can be directed on the channel's inlet as shown in "Figure 1".

Due to the relatively high absorptivity (α) value of the ceramic catalyst material used in the HiTRec absorber in the range 0.9-0.96 [6], the largest portion of the incident radiation which penetrates the receiver is directly absorbed when it strikes the inner walls of the channel. The amount left is reflected and is subjected to multiple absorption/reflection [13] between the SiC walls of the channel, which are assumed to be gray [15] diffusely reflecting surfaces in this study.
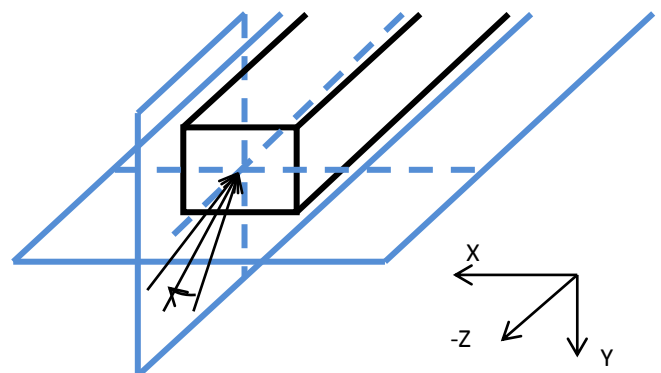

Fig. 1. Schematic of solar beams striking the channel's inlet at different angles of incidence in the y-z plane

In order to consider for the phenomenon of multiple absorption/reflection, the discrete ordinates (DO) radiative model has been used. The (DO) radiative model divides the hemisphere surrounding an emitting wall element to a finite number of solid angles (Ω), each associated with a vector direction $(\vec{s})$ fixed in a global Cartesian system. The (DO) radiative model solves the RTE for every radiation intensity (I_{out}) and (I_{in}) assigned to a direction vector [16]. The idea of using the (DO) radiative model is its boundary condition capable of considering for the multiple absorption/reflection occurring between the channel's walls, where the net radiative flux leaving a surface (q_{out}) in the (DO) radiative model is given in [17] as the wall's thermal emission due to the wall temperature and the reflected amount from the incident radiative flux (q_{in}) which is either coming from the surrounding walls and/or from the direct concentrated solar flux $(\overline{G_{0-n}})$ penetrating the channel. The radiative flux (q_{abs}) is the amount absorbed from the incident radiative flux (q_{in}).

The schematic of the study case is shown in "Figure 2". And the dimensions of the cross sectional cut in the REV are given in "Figure 3".
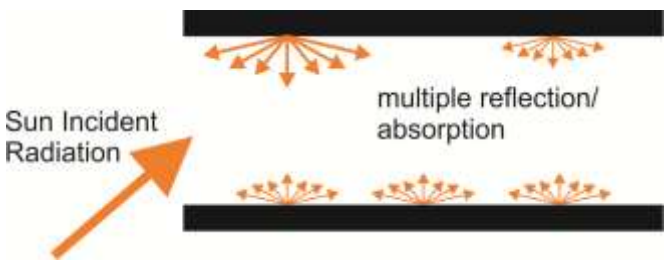

Fig. 2. Longitudinal section in the REV under solar load
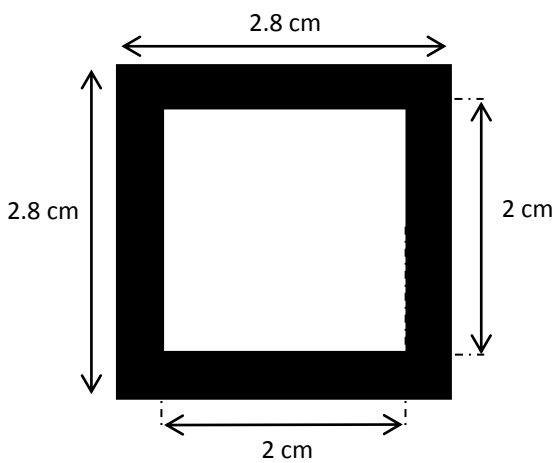

Fig. 3. Dimensions of the cross section in the REV (solid is marked in black)

The REV volume consists of two phases (solid and fluid phases) with a porosity (P_0) of 0.51 [13] and a depth of 5 cm [18]. The fluid used for heat exchange is air. In an absorbing-scattering medium, the extinction coefficient (β) consists of an absorption coefficient (κ) that describes how radiative energy is converted to internal energy of the matter and a scattering coefficient (σ) representing the change of the direction of radiation propagating with no radiative energy converted to thermal energy [16]. The extinction coefficient (β) is therefore expressed as, $\beta = \kappa + \sigma$. The radiative flux which penetrates the channel is converted to thermal energy absorbed by the walls either from the first strike or after multiple absorption/reflection. Only a slight amount of the reflected radiation escapes from the inlet. This radiation loss has been quantified and it amounts for less than 1% of the incident radiative flux for any incident angle. It has been therefore neglected in this study. This can simplify any honeycomb structure (enclosure) to an absorbing medium of the incident flux with no need for a scattering coefficient (σ), hence, $\kappa = \beta$ and $\sigma = 0$.

The geometry of interest in the simulation is the fluid volume (air) with defined wall boundaries because absorptivity (α) and reflectivity (ρ) are properties at the interfaces [16] and the heat conduction in the solid is not studied in this work. The wall thickness is therefore of no interest in the model. The channel inlet and outlet shown in "Figure 4" are defined as semitransparent wall boundaries with a transmissivity (τ) value of 1, to make no interaction with the striking beam as the air in the channel is treated as non-participating medium [16]. The side walls are approximated to be opaque diffused gray walls having a total hemispherical absorptivity (α) of 0.93. The temperature (T) of all walls is identical and fixed as the heat transfer due thermal emission is not studied in this work. This is the case when the incident radiation strikes the unheated receiver at the start of operation.
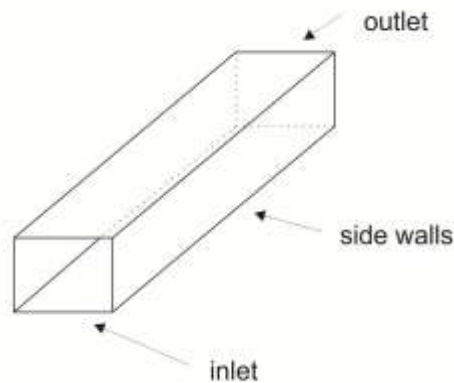

Fig. 4. Air volume boundaries

A solar load with an arbitrary angle of incidence ($\theta_n = 30°$) striking the channel's inlet is shown in "Figure 5". The total absorbed flux (q_{abs}), after multiple absorption/reflection inside the channel, is available for all walls as one of the simulation results.

In order to find the extinction coefficient (β_n) of the solar radiation ($\overline{G_{0-n}}$) striking the channel's inlet with this angle of incidence ($\theta_n = 30°$), the first step is to divide the channel into a number of slices (20 slices have been used in this work). "Figure 6" highlights one of the 20 slices dividing the channel (19 slices are hidden for the purpose of demonstration). The total power absorbed in any slice (Q_{abs}) is the summation of the power absorbed by each of the 4 elemental walls forming a slice. When the total absorbed thermal power (Q_{abs}) inside a slice is divided by the slice volume (V), the result is an *average* absorbed power per unit volume (Q_{vol}). Performing the same operation for each slice leads to the graph shown in "Figure 7", which is the *average* absorbed power per slice volume (Q_{vol}) in each slice along the axial coordinate (z) of the channel when subjected to solar radiation ($\overline{G_{0-n}}$) at an angle of incidence ($\theta_n = 30°$). The volumetric absorbed power graph is the key to find the extinction coefficient (β), as the attenuation graph can be obtained by integrating the (Q_{vol}) graph with respect to (z) as previously demonstrated in "equation (1)" and "equation (3)".

The channel's depth studied is 10 mm and the slice volume (V) includes the solid and fluid phases and equals 3.92 mm³.
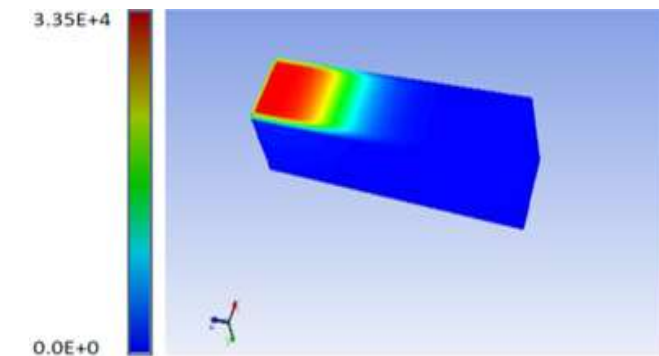
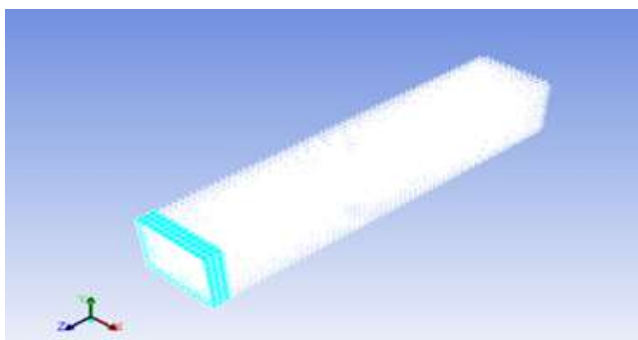**Fig. 5.** Total absorbed radiative flux (q_{abs}) available for all walls [W/m²]

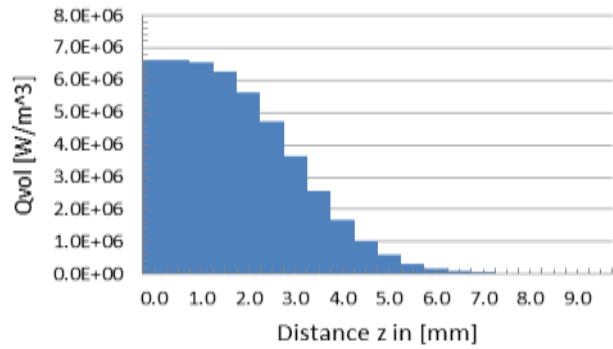**Fig. 6.** The 4 elemental walls forming a channel's slice

Fig. 7. Average absorbed power per slice volume (Q_{vol}) along the axial coordinate (z) of the channel at a ($\theta_n = 30°$).

A new honeycomb geometry has been investigated in this study. The novel geometry is divided into two parts. The first part receiving the radiation has higher porosity (P_0) of 0.75 to allow for more radiation penetration inside the volume and side holes for better fluid mixing. The front and side views of the first body are given in "Figure 8". The second part is identical to the previously studied channel. A schematic showing the longitudinal side view of the channel is given in "Figure 9". The same solar load at the same angle of incidence ($\theta_n = 30°$) is simulated for the novel channel and the result is shown in "Figure 10". The total absorbed flux (q_{abs}), after multiple absorption/reflection inside the channel is available for all walls. As the radiative flux is absorbed in the first few millimeters in both geometries, shorter lengths have been defined in the simulation.

A similar graph for the volumetric absorbed power (Q_{vol}) along the axial coordinate of the channel (z) is shown in "Figure 11". The side holes are defined as walls with specular reflection because the amount of radiation leaving the side holes of a channel is equal to the amount entering from neighboring side channels as shown in "Figure 12".

The channels depth studied is 10 mm and the slice volume (V) includes the solid and fluid phases and equals 3.92 mm³.The solar load is found in "Table 2" and "Table 3" for n=3.
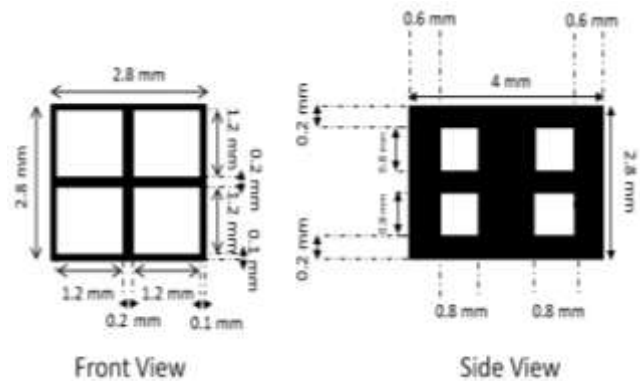
Fig. 8. Front and side views of the first part of the novel channel (solid is marked in black)
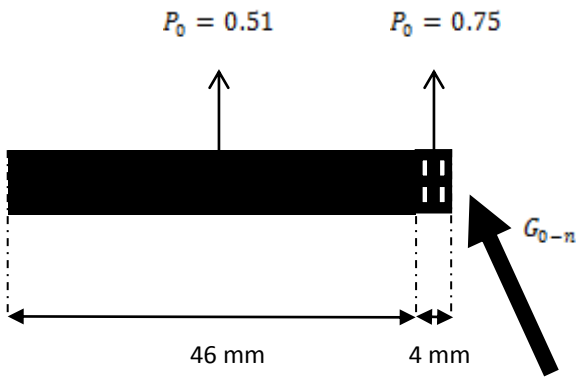
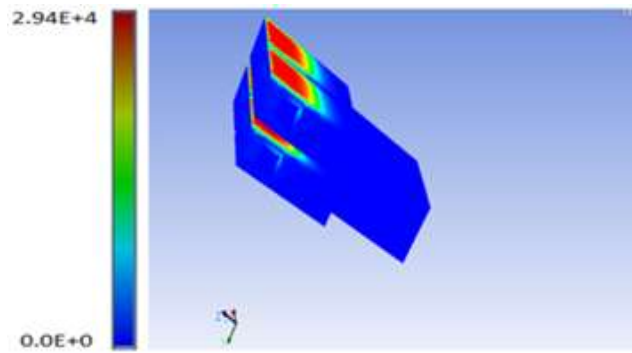**Fig. 9.** Longitudinal side view of the novel channel

Fig. 10. Absorbed radiative flux (q_{abs}) in the novel channel available for all walls [W/m^2]
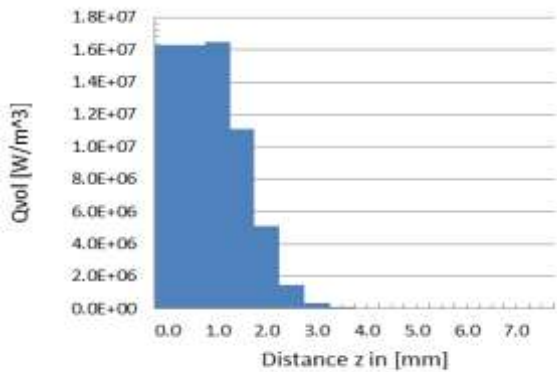

Fig. 11. Average absorbed power per slice volume (Q_{vol}) along the axial coordinate (z) of the novel channel ($\theta_n = 30°$)
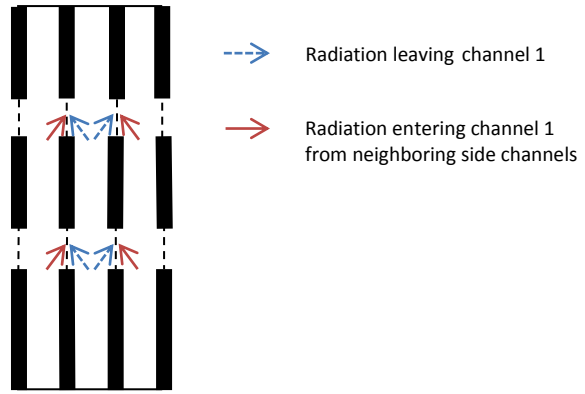

Fig. 12. Longitudinal cut through the side holes inside the novel channel

3. Results

In this study, 15 angles of the solar radiative flux ($\overline{G_0}$) are considered to be incident on the inlet, as a compromise between good discretization and computational time. A schematic is shown in "Figure 13". The angles of incidence investigated are given in "Table 1". A total solar radiative flux of 800 [$\frac{KW}{m^2}$] is assumed to be reflected from the heliostat field [19]. This total flux density is divided by the number of angles (n =15), each entity is then multiplied by its corresponding $cos(\theta_n)$ to find the normal solar radiative flux (G_{0-n}) for every angle of incidence (θ_n) as shown in "Table 2" and "Table 3".

The total average volumetric absorbed power ($\sum_{n=1}^{15} Q_{vol}$) is given in "Figure 14" and "Figure 15" for both geometries. The attenuation graph of the total incident normal radiative flux ($[\sum_{n=1}^{15} G_{0-n}].P_0$) is found by the integration of ($\sum_{n=1}^{15} Q_{vol}$) with respect to (z) and is given in "Figure 16" and "Figure 17".
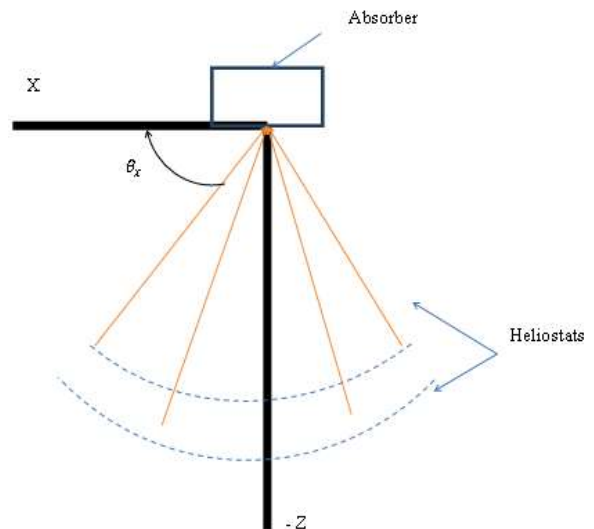

Fig. 13. Representation of the heliostats' field with a smaller number of beams (top view)

Table 1. Angles of incidence investigated

n	θ_x	θ_y	θ_z
1	90°	90°	0°
2	90°	75°	15°
3	90°	60°	30°
4	75°	90°	15°
5	75°	75°	15°
6	75°	60°	15°
7	60°	90°	30°
8	60°	75°	30°
9	60°	60°	30°
10	105°	90°	-15°
11	105°	75°	-15°
12	105°	60°	-15°
13	120°	90°	-30°
14	120°	75°	-30°
15	120°	60°	-30°

The angles in "Table 1" are defined by an angle number (n) and by θ_x, θ_y and θ_z according to the cartesian coordinate system shown in "Figure 13". "Table 2" and "Table 3" show the available normal radiative flux at the inlet of the two investigated channels for each incident angle. The summation of the 15 values gives the total normal radiative flux available at the inlet of the channel. The tables also show the amount of normal radiative flux lost through the inlet by the walls' reflection. It can be seen from "Table 2" and "Table 3" that the amount of the reflected radiation escaping from the inlet is relatively small when compared to the incident flux on the inlet. It has therefore been neglected in the study.

Table 2. Normal radiative flux (G_{0-n}) at the inlet of the HiTRec channel and the corresponding normal flux lost

n	$G_{0-n} \cdot P_0 \; [\frac{W}{m^2}]$	$G_{0-n-L} \cdot P_0 \; [\frac{W}{m^2}]$
1	27199	0
2	26273	123
3	25298	164
4	26273	123
5	25377	192
6	22753	249
7	25298	164
8	22753	251
9	20400	273
10	26273	123
11	25377	192
12	22753	249
13	25298	164
14	22753	251
15	20400	273
$P_0 \cdot \sum_{n=1}^{15} G_{0-n-(L)}$	364484	2800

Table 3. Normal radiative flux (G_{0-n}) at the inlet of the novel channel and the corresponding normal flux lost.

n	$G_{0-n} \cdot P_0 \ [\frac{W}{m^2}]$	$G_{0-n-L} \cdot P_0 \ [\frac{W}{m^2}]$
1	39183	88
2	37848	211
3	33934	328
4	37848	226
5	36558	317
6	32777	390
7	33934	325
8	32777	387
9	29387	401
10	37848	226
11	36558	317
12	32777	390
13	33934	325
14	32777	387
15	29387	401
$P_0 \cdot \sum_{n=1}^{15} G_{0-n-(L)}$	364484	2800

The total available normal radiative flux at the inlet is absorbed and the result is the total power absorbed (Q_{abs}) per each slice of the channel given in "Figure 14" and "Figure 15".
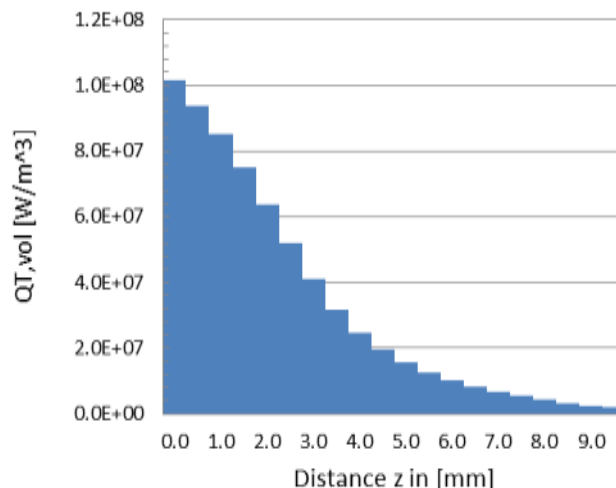

Fig. 14. Total average absorbed power per volume $(Q_{T,vol})$ inside the HiTRec channel due to flux striking the receiver at 15 different angles
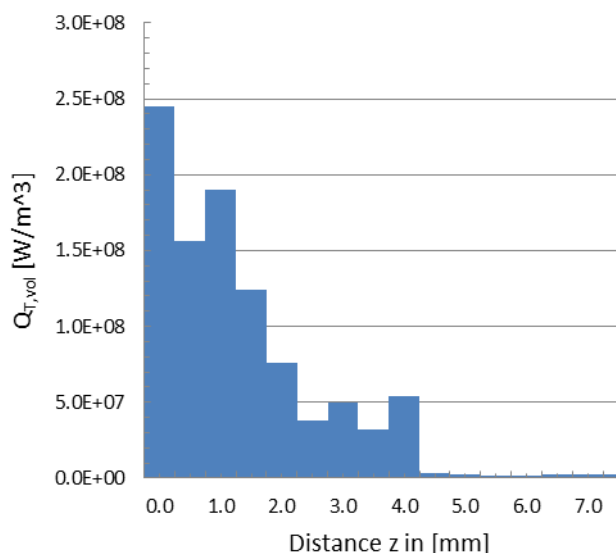

Fig. 15. Total average absorbed power per volume $(Q_{T,vol})$ inside the novel channel due to flux striking the receiver at 15 different angles

The total average absorbed power per volume $(Q_{T,vol})$ graphs lead to the attenuation graphs given in "Figure 16" and "Figure 17" from which the extinction coefficient (β) is deduced.
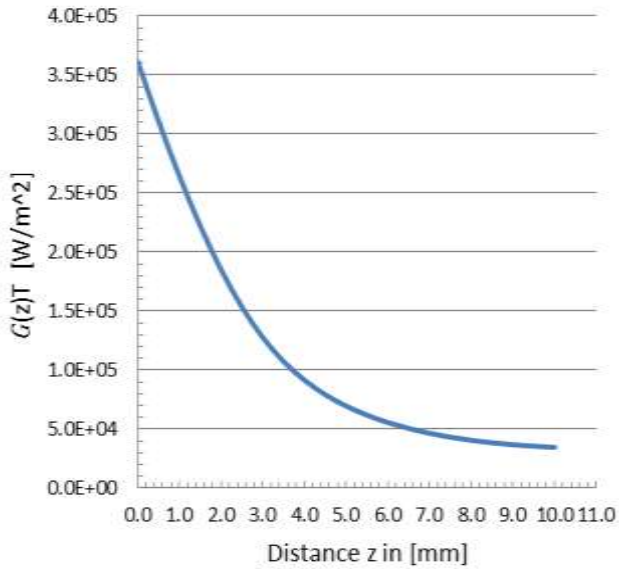
Fig. 16. Attenuation graph of the total incident normal radiative flux $\left(\sum_{n=1}^{15} P_0 \cdot G_{0-n}\right)$ inside the HiTRec channel

exponential approximation with a constant extinction coefficient $(\beta_{\sum n})$ of the attenuation curve in the HiTRec channel is given in "Figure 18". The constant extinction coefficient $(\beta_{\sum n})$ has a value of $234.7 \frac{1}{m}$.

A more accurate approximation of the attenuation graph is done via an extinction coefficient $(\beta_{\sum n})$ of polynomial nature where,

$$\beta_{\sum n}(z) = -3 \times 10^6 \, z^2 - 1198.6 \, z + 324.74$$

The approximation with a polynomial extinction coefficient (β) compared to the constant extinction coefficient (β) approximation is given in "Figure 19". It has to be noted that the radiation is absorbed in the first 10 mm of the channel. The solar radiative flux (G_{0-1}) at the angle of incidence (θ_1) will pass through the channel unaffected.

The REV of the novel geometry is subjected to the same angles of incidence as in the HiTRec channel. The attenuation curve and its constant exponential approximation are given in "Figure 20". The constant extinction coefficient (β) has a value of $546.7 \frac{1}{m}$.
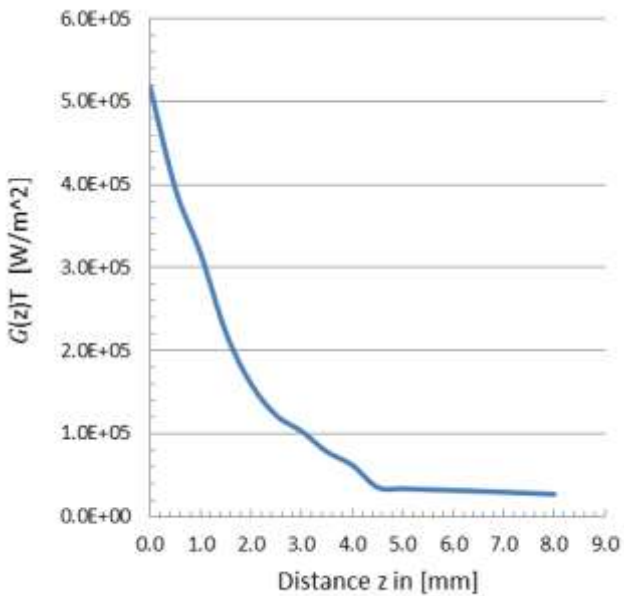

Fig 17. Attenuation graph of the total incident normal radiative flux $\left(\sum_{n=1}^{15} P_0 \cdot G_{0-n}\right)$ inside the novel channel
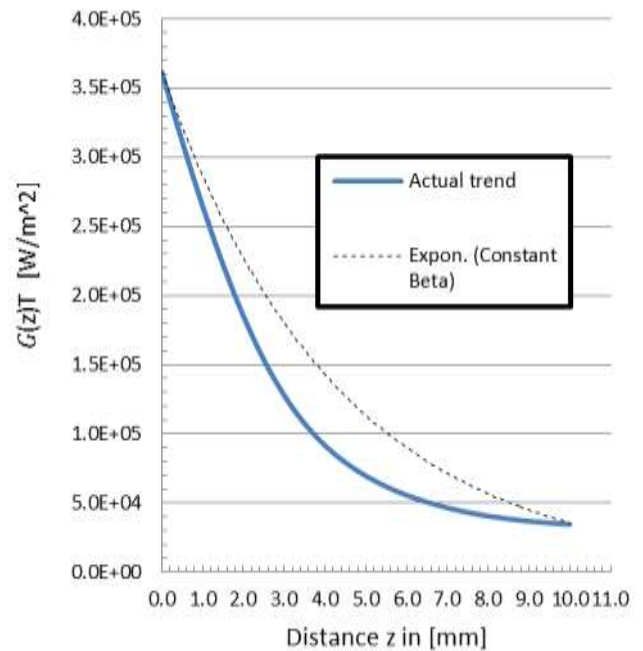

Fig. 18. Constant exponential approximation of the attenuation graph of the total incident normal radiative flux $\left(\sum_{n=1}^{15} P_0 \cdot G_{0-n}\right)$ inside the channel

The important findings of this study are: 1) Showing that a honeycomb pattern can be treated as an absorbing medium. 2) Providing a numerical tool to evaluate the effective radiative parameter for honeycomb patterns. 3) Showing that the assumption of a constant extinction coefficient $(\beta_{\sum n})$ of the incident radiation is not always a valid assumption and can include a significant error. The
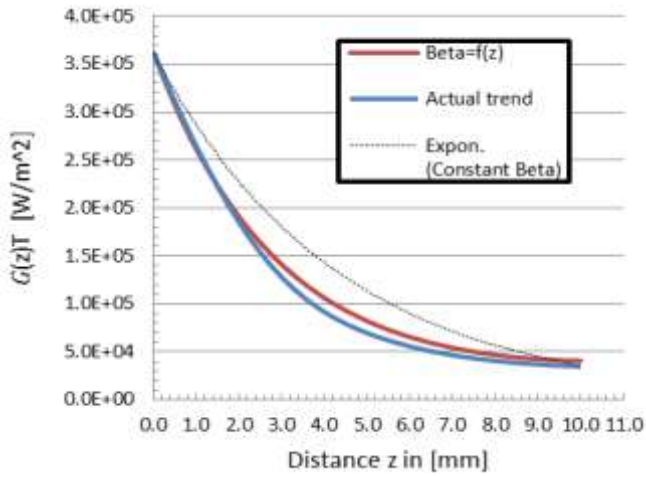
Fig. 19. The exponential approximation of the $(G(z)_T)$ inside the HiTRec channel – Constant and z-dependent extinction coefficient (β) approximations
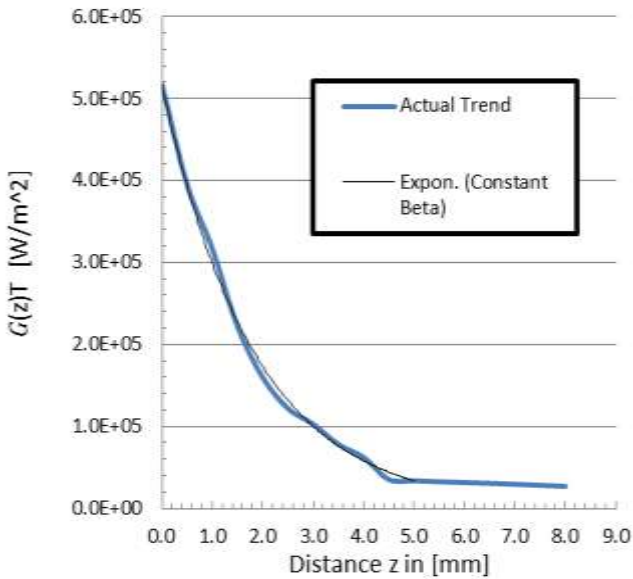

Fig. 20. The exponential approximation of the $(G(z)_T)$ inside the novel geometry.

Finally, the attenuation graphs $(G(z)_T)$ of the total incident

normal radiative flux inside the two geometries are reported in "Figure 21". As previously expected, the novel structure with the higher porosity (P_0) at the inlet allows for higher

penetration of the incident radiative flux at the inlet. The attenuation of the radiation inside the channel gives the extinction coefficient (β): one of the input parameters

needed to run a continuum model simulation of the complete receiver module to be able to decide for the structure which offers a higher solar-to-thermal efficiency (η).
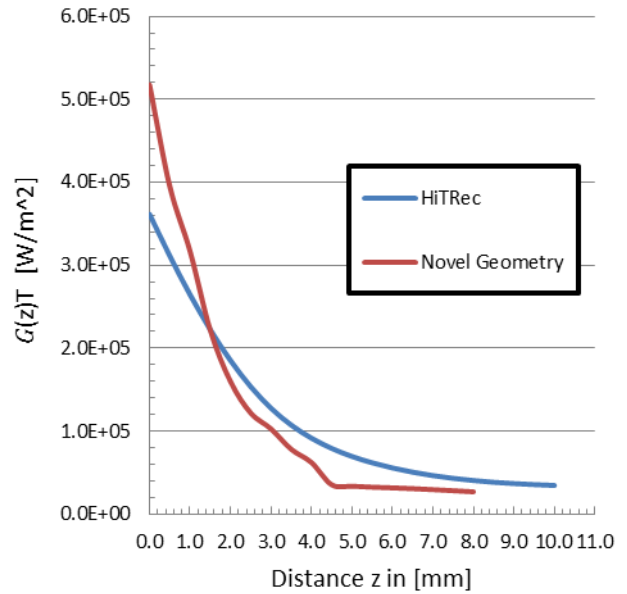

Fig. 21. Attenuation graphs $(G(z)_T)$ inside the studied

geometries.

3. Conclusion

This study presents a technique for evaluating the extinction coefficient (β) of honeycomb structures. It has

been demonstrated in the study that a honeycomb structure can be modeled as an absorbing medium. This simplifies the extinction coefficient (β) of a honeycomb geometry to an

absorption coefficient (κ) and eliminates the need for a

scattering coefficient (σ).

The developed tool is used to determine the absorbed radiation profile in any proposed honeycomb shape when the rays hit the cool receiver at the start of operation. A heliostat field has been simplified by a number of rays at different incident angles hitting the inlet of two different geometries. The results deduced show that the extinction coefficient (β)

of a honeycomb structure can be approximated to a constant or a polynomial function.

In order to compare between the solar-to-thermal efficiencies (η) of the different honeycomb geometries used

as solar receivers, a continuum model simulation where heat and flow equations are coupled must be performed. For that purpose, all the effective parameters representing the physical phenomena occurring in a porous receiver have to be available and the radiation losses to the atmosphere through the inlet opening due to the thermal emission of the walls when the receiver is heated up has to be considered.

NOMENCLATURE

Greek Symbols

β	Extinction coefficient [m^{-1}]
κ	Absorption coefficient [m^{-1}]
σ	Scattering coefficient [m^{-1}]
α	Hemispherical total absorptivity
τ	Hemispherical total transmissivity
ρ	Hemispherical total reflectivity
Ω	Solid angle [sr]
η	Solar-to-thermal efficiency
θ	Angle of incidence [degrees]
θ_x	Angle between beam and x axis [degrees]
θ_y	Angle between beam and y axis [degrees]
θ_z	Angle between beam and the negative z axis [degrees]

Latin Symbols

P_0	Porosity (%)
G_0	Normal flux at the receiver's inlet [W.m^{-2}]
$\overline{G_0}$	Solar flux striking the receiver's inlet at an angle of incidence [W.m^{-2}]
A_v	Specific Surface Area [m^2.m^{-3}]
V	Volume [m^3]
h	Heat Transfer Coefficient [W.m^{-2}.K]
T	Temperature [k]
z	Z axis in the main axial air flow direction [m]
I_{in}	Radiation intensity incident on a wall [W. m^{-2}.sr^{-1}]
I_{out}	Radiation intensity leaving a wall [W. m^{-2}.sr^{-1}]
q_{in}	The net radiative flux incident on a wall [W. m^{-2}]
q_{out}	The net radiative flux leaving a wall [W. m^{-2}]
q_{abs}	The radiative flux absorbed by a wall [W. m^{-2}]
Q_{abs}	Absorbed thermal power [W]
Q_{vol}	Absorbed thermal power per unit volume [W.m^{-3}]
$\vec{s}$	Direction vector assigned to a specific discrete solid angle

Subscripts

n	Number assigned to an angle of incidence
L	Loss
0	Inlet
T	Total

Abbreviations

REV	Representative Elemental Volume
RTE	Radiative Transfer Equation
DO	Discrete Ordinate
HiTRec	High Temperature Receiver

References

[1] T. Fend, "High Porosity Materials as Volumetric Receivers for Solar Energetics", Optica Applicata, vol. 40, pp. 271–284, 2010.

[2] R. Capuano, T. Fend, P. Schwarzbözl, O. Smirnova, H. Stadler, B. Hoffschmidt, "Numerical models of advanced ceramic absorbers for volumetric solar receivers", Renewable and Sustainable Energy Reviews, vol. 58, pp. 656–665, 2016.

[3] R. Capuano, T. Fend, B. Hoffschmidt, R. Pitz-Paal, "Innovative Volumetric Solar Receiver Micro-Design Based on Numerical Predictions" ASME 2015 International Mechanical Engineering Congress and Exposition, vol. 8B: Heat Transfer and Thermal Engineering, Houston, Texas, USA, November 13–19, 2015.

[4] B. Hoffschmidt, V. Fernández, A.G. Konstandopoulos, I. Mavroidis, M. Romero, P. Stobbe, F.Téllez,"Development of Ceramic Volumetric Receiver Technology", Proc. of 5th Cologne Solar Symp., June 2001; K.-H. Funken and W. Bucher, eds. Forschungsbericht 2001–10, DLR-Cologne, Germany, pp. 51–61.

[5] B. Hoffschmidt, Téllez Félix M., A. Valverde, J. Fernández, V. Fernández, "Performance Evaluation of the 200-kW[th] HiTRec-II Open Volumetric Air Receiver", J. Sol. Energy Eng., vol. 125, pp. 87–94, 2003.

[6] T. Fend, B. Hoffschmidt, R. Pitz-Paal, O. Reutter, P. Rietbrock, "Porous materials as open volumetric solar receivers: Experimental determination of thermophysical and heat transfer properties", Energy, vol. 29, pp. 823–833, 2004.

[7] T. Fend, R. Pitz-Paal, O. Reutter, J. Bauer, B. Hoffschmidt, "Two novel high-porosity materials as volumetric receivers for concentrated solar radiation", Solar Energy Materials and Solar Cells, vol. 84, pp. 291–304, 2004.

[8] R. Capuano, "Comprehensive numerical approach for the design and optimization of solar absorber microstructures", 10th Sollab Doctoral Colloquium on Solar Concentrating Technologies, Odeillo - Font Romeu, 23–25 June 2014.

[9] V. Jambhekar, "Forchheimer porous-media flow models- numerical investigation and comparison with

experimental data", Master Thesis, University of Stuttgart; 2011.

[10] J. Mils, "A continuum approach to two-phase porous media", Transport in porous media, vol. 35, pp. 15–36, 1999.

[11] J. Petrasch, S. Haussener, W. Lipinski,"Discrete vs. continuum-scale simulation of radiative transfer in semitransparent two-phase media", Journal of Quantitative Spectroscopy and Radiative Transfer, 112(9), pp. 1450–1459, 2011.

[12] C. Caliot, Z. Wu, G. Flamant, Z. Wang, "Numerical simulation of convective heat transfer between air flow and ceramic foams to optimize volumetric solar air receiver performances", International Journal of Heat and Mass Transfer, 54(7-8), pp.1527–1537, 2011.

[13] T. Fend, R. Pitz-Paal, B. Hoffschmidt, O. Reutter, "Solar radiation conversion", in: "Cellular Ceramics: Structure, Manufacturing, Properties and Applications" (eds. M. Scheffler and P. Colombo), Wiley-VCH, Weinheim, 2005.

[14] T. Fend, P. Schwarzbözl, O. Smirnova, D. Schöllgen, C. Jakob, "Numerical investigation of flow and heat transfer in a volumetric solar receiver", Renewable Energy, vol. 60, pp. 655–661, 2013.

[15] S. Mey, C. Caliot, G. Flamant, A. Kribus, Y. Gray, "Optimization of High Temperature SiC Volumetric Solar Absorber", Energy Procedia, vol. 49, pp. 478–487, 2014.

[16] R. Siegel, J. Howell, M. Menguc, Thermal radiation heat transfer, 5th ed, Taylor & Francis, 2010.

[17] Reference Manual, FLUENT 6.3, Discrete Ordinates (DO) Radiation Model Theory.

[18] O. Smirnova, T. Fend, S. Peter, D. Schöllgen, "Homogeneous and Inhomogeneous Model for Flow and Heat Transfer in Porous Materials as High Temperature Solar Air Receivers", European COMSOL Conference, Paris, 17-19 November 2010.

[19] G. Koll, P. Schwarzbözl, K. Hennecke, T. Hartz, M. Schmitz, B. Hoffschmidt, "The solar tower Jülich—A research and demonstration plant for central Receiver Systems", SolarPACES Conference, Berlin, 15-18 September 2009.